Molecular Crystals and Liquid Crystals
Publication details, including instructions for authors and subscription information:
http://www.tandfonline.com/loi/gmcl16

# Local Refractive Index Measurement on a Cholesteric Liquid Crystal Using the Surface Plasmon Technique

Nan-Ming Chao [a b], K. C. Chu [a] & Y. R. Shen [a]
[a] Department of Physics, University of California, Berkeley, California, 94720, U.S.A.
[b] Tsinghua University, Beijing, China
Version of record first published: 14 Oct 2011.

*Mol. Cryst. Liq. Cryst.*, 1981, Vol. 67, pp. 261–276
0026–8941/81/6704–0261$06.50/0




# Local Refractive Index Measurement on a Cholesteric Liquid Crystal Using the Surface Plasmon Technique†

NAN-MING CHAO‡, K. C. CHU§ and Y. R. SHEN

*Department of Physics, University of California, Berkeley, California, U.S.A. 94720*

(*Received July 10, 1980*)

The surface plasmon technique is used to measure the local refractive indices in the quasi-nematic layers of a cholesteric liquid crystal with an accuracy of about $10^{-4}$. The local linear birefringence reflecting the orientational order of molecules in the quasi-nematic layers shows a temperature dependence characteristic of a nematic and in good agreement with the theory of nematic ordering.

## I INTRODUCTION

Reports on refractive index and optical birefringence measurements of liquid crystals have appeared frequently in recent literatures,[1] but few of them deal with materials in the cholesteric phase. This is presumably because of the difficulty in extracting the "local" refractive indices from the measured quantities, owing to the helical structure of the cholesterics. The information of the local refractive indices in a plane perpendicular to the helical axis is nevertheless very important, since the corresponding linear birefringence reflects the orientational ordering of molecules in that plane.

Several methods have been proposed to determine refractive indices (or birefringence) of cholesteric liquid crystals, namely, the Abbe refractometer method,[2–5] the optical rotatory dispersion (ORD) method,[6, 7] snd the circular dichroism (CD) method.[8] Each method has its advantages and disadvantages

† Research supported by the National Science Foundation, Grant DMR78-18826.
‡ On leave from Tsinghua University, Beijing, China.
§ Permanent address: Bell Laboratories, Murray Hill, New Jersey.
Paper presented at the 8th International Liquid Crystal Conference, Kyoto, Japan, June 30–July 4, 1980.

as will be discussed later. We propose here the surface plasmon technique which allows us to determine the local refractive indices of a cholesteric to an accuracy of $\lesssim 10^{-4}$, clearly better than the other techniques. It has recently been applied to the measurements of refractive indices of a nematic material and to the study of the nematic-isotropic phase transition.[9]

The sample, arbitrarily chosen, was a mixture of cholestryl chloride and cholesteryl myristate (1.75:1 by weight). In the cholesteric phase, it changes with temperature from left to right helical structure with its pitch changing continuously from $-2.82$ $\mu$m to $\infty$ to 1.75 $\mu$m. However, if the cholesteric phase can be regarded as a pile of thin quasi-nematic layers stacked into a helical structure, then the variation of the local refractive indices with temperatures should resemble that of a nematic with an abrupt change occurring at the cholesteric-isotropic transition. Indeed, this is what we have observed. Our results of local linear birefringence for the cholesteric as a function of temperature are in excellent agreement with the molecular field theory for the temperature variation of the nematic order parameter.

In Section II, we first present the theoretical background of the surface plasmon technique. Then, in Sections III and IV, the experimental arrangement and results are described. Finally, in Section V, the results are studied in terms of the theories of molecular orientational ordering for nematics and various techniques for refractive index measurements are compared and discussed.

## II THEORY

A surface plasmon is a transverse magnetic electromagnetic wave travelling along the interface between a metal and a dielectric.[10] It decays exponentially in directions normal to the interface with decay lengths of the order of $\lambda/\pi$, where $\lambda$ is the wavelength in the boundary media, so that its propagation characteristics are quite sensitive to the interface structure, and can therefore be used for accurate measurements of the optical constants of boundary media,[11,12] overlayers, and adsorbed molecular species on metal surfaces.[13,14] In our experiment, we used the Kretschmann's scheme[11] to excite the surface plasmon on an interface between the metal and the cholesteric, as shown in Figure 1. The reflected TM wave was monitored as a function of the incident angle. The resulting reflectivity curve was then fit by the theory described below, and the refractive indices were deduced.

We consider a single-domain cholesteric liquid crystal with its helical axis along the normal of the interface $\hat{z}$. The plane of incidence is $\hat{x}$–$\hat{z}$ and

the beam polarization is in the same plane (TM mode). According to the Oseen's model,[15] the dielectric property of a cholesteric can be described macroscopically by a spiralling dielectric tensor. In a reference frame, with coordinates $\xi$, $\eta$ and $z$, spiralling with the helical structure, the dielectric tensor is diagonalized:

$$\overleftrightarrow{\epsilon}_T = \begin{pmatrix} \epsilon_\xi & 0 & 0 \\ 0 & \epsilon_\eta & 0 \\ 0 & 0 & \epsilon_z \end{pmatrix}. \tag{1}$$

The corresponding dielectric tensor in the laboratory coordinates is

$$\overleftrightarrow{\epsilon}_L = \begin{pmatrix} \bar{\epsilon} + \delta \cos 2\beta z & \delta \sin 2\beta z & 0 \\ \delta \sin 2\beta z & \bar{\epsilon} - \delta \cos 2\beta z & 0 \\ 0 & 0 & \epsilon_z \end{pmatrix} \tag{2}$$

where

$$\bar{\epsilon} = \tfrac{1}{2}(\epsilon_\xi + \epsilon_\eta)$$
$$\delta = \tfrac{1}{2}(\epsilon_\xi - \epsilon_\eta)$$
$$\beta = \frac{2\pi}{P} \tag{3}$$

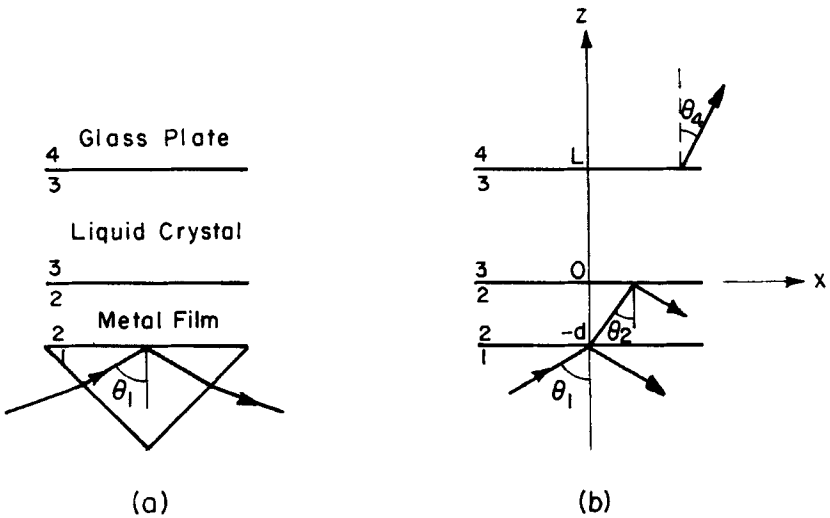


FIGURE 1 Schematic of the sample assembly.

and $P$ is the helical pitch. In our experiment, the local directors of molecular ordering in the $z = 0$ and $z = L$ planes were aligned parallel to $\hat{y}$ so that

$$\epsilon_z \approx \epsilon_\xi = (n_\perp)^2$$
$$\epsilon_\eta = (n_\parallel)^2, \tag{4}$$

with $n_\perp$ and $n_\parallel$ being respectively the refractive index components perpendicular and parallel to the local director in the quasi-nematic layers.

The helical structure of the cholesteric phase significantly complicates the calculation of the reflectivity for the multi-layer system with obliquely incident light shown in Figure 1. The result of reflectivity versus the angle of incidence $\theta_1$ can however be cast into the form

$$R^{pp}(\theta_1) = \left| \frac{[\gamma_{12}^{pp} + \gamma_{23}^{pp}\exp(i2k_{2z}d)][1 + \gamma_{12}^{ss}\gamma_{23}^{ss}\exp(i2k_{2z}d)] - \gamma_{12}^{ss}\gamma_{23}^{ps}\gamma_{23}^{sp}\exp(i4k_{2z}d)}{[1 + \gamma_{12}^{pp}\gamma_{23}^{pp}\exp(i2k_{2z}d)][1 + \gamma_{12}^{ss}\gamma_{23}^{ss}\exp(i2k_{2z}d)] - \gamma_{12}^{pp}\gamma_{12}^{ss}\gamma_{23}^{ps}\gamma_{23}^{sp}\exp(i4k_{2z}d)} \right|^2. \tag{5}$$

Here, the superscripts $p$ and $s$ refer to the TM and TE polarizations respectively, the subscripts 1, 2, 3, and 4 denote the prism, metal film, cholesteric liquid crystal, and glass plate, $k_{iz}$ is the $z$ component of the wavevector in the $i$th medium and is related to the $x$-component of the wavevector $k_x = k_i \sin\theta_i$ by $k_x^2 + k_{iz}^2 = (\omega/c)^2 n_i^2$, $d$ is the thickness of the metal film, and $\gamma_{ij}^{\mu\nu}$ is the Fresnel reflection coefficient at the $i$-$j$ interface with incident and reflected beam polarizations being $\nu$ and $\mu$ respectively. We have

$$\gamma_{12}^{pp} = \frac{(n_2^2 k_{1z} - n_1^2 k_{2z})}{(n_2^2 k_{1z} + n_1^2 k_{2z})}, \tag{6}$$

$$\gamma_{12}^{ss} = \frac{(k_{1z} - k_{2z})}{(k_{1z} + k_{2z})}. \tag{7}$$

Similar expressions are expected for $\gamma_{23}^{pp}$ and $\gamma_{23}^{ss}$ with $\gamma_{23}^{sp} = \gamma_{23}^{ps} = 0$ if the dielectric tensor of medium 3 is spatially invariant and diagonal; then Eq. (5) reduces to the familiar form:

$$R^{pp}(\theta_1) = \left| \frac{\gamma_{12}^{pp} + \gamma_{23}^{pp}\exp(i2k_{2z}d)}{1 + \gamma_{12}^{pp}\gamma_{23}^{pp}\exp(i2k_{2z}d)} \right|^2.$$

In the case of a cholesteric phase for medium 3, however, not only $\gamma_{23}^{ps}$ and $\gamma_{23}^{sp}$ are nonvanishing but no analytical expressions exist for $\gamma_{23}^{pp}$, $\gamma_{23}^{ss}$, $\gamma_{23}^{ps}$ and $\gamma_{23}^{sp}$. Yet they can be found numerically following Taupin,[16] and Berreman and Scheffer.[17] We use here the latter's matrix multiplication method.

The results are given by

$$\gamma_{23}^{pp} = \frac{(B_1C_2 - A_2D_1)}{(A_1C_2 - A_2C_1)}, \tag{8a}$$

$$\gamma_{23}^{ps} = \frac{(B_2C_2 - A_2D_2)}{(A_1C_2 - A_2C_1)}, \tag{8b}$$

$$\gamma_{23}^{sp} = \frac{(A_1D_1 - C_1B_1)}{(A_1C_2 - A_2C_1)}, \tag{8c}$$

$$\gamma_{23}^{ss} = \frac{(A_1D_2 - C_1B_2)}{(A_1C_2 - A_2C_1)}. \tag{8d}$$

where

$$A_1 = \left[\frac{n_2n_4F_{12}}{\cos\theta_4\cos\theta_2)} - F_{21} + i\left(\frac{n_4F_{11}}{\cos\theta_4} + \frac{n_2F_{22}}{\cos\theta_2}\right)\right], \tag{9a}$$

$$A_2 = \left[\frac{n_2n_4\cos\theta_2F_{14}}{\cos\theta_4} - F_{23} + i\left(\frac{n_4F_{13}}{\cos\theta_4} + n_2F_{24}\cos\theta_2\right)\right], \tag{9b}$$

$$B_1 = \left[\frac{n_2n_4F_{12}}{\cos\theta_4\cos\theta_2} + F_{21} + \mathrm{i}\left(\frac{n_2F_{22}}{\cos\theta_2} - \frac{n_4F_{11}}{\cos\theta_4}\right)\right], \tag{9c}$$

$$B_2 = \left[\frac{n_2n_4F_{14}\cos\theta_2}{\cos\theta_4} + F_{23} + i\left(\frac{n_2F_{24}\cos\theta_2 - n_4F_{13}}{\cos\theta_4}\right)\right], \tag{9d}$$

$$C_1 = \left[\frac{n_2n_4F_{32}\cos\theta_4}{\cos\theta_2} - F_{41} + i\left(\frac{n_4F_{31}\cos\theta_4 + n_2F_{42}}{\cos\theta_2}\right)\right], \tag{9e}$$

$$C_2 = [n_2n_4F_{34}\cos\theta_2\cos\theta_4 - F_{43} + i(n_4F_{33}\cos\theta_4 + n_2F_{44}\cos\theta_2)], \tag{9f}$$

$$D_1 = \left[\frac{n_2n_4F_{32}\cos\theta_4}{\cos\theta_2} + F_{41} + i\left(\frac{n_2F_{42}}{\cos\theta_2 - n_4F_{31}\cos\theta_4}\right)\right], \tag{9g}$$

$$D_2 = [n_2n_4F_{34}\cos\theta_2\cos\theta_4 + F_{43} + i(n_2F_{44}\cos\theta_2 - n_4F_{33}\cos\theta_4)], \tag{9h}$$

$F_{ij}$ are the elements of the 4 × 4 propagation matrix $\mathbb{F}(0, L)$, which has the form

$$\mathbb{F}(O, L) \approx \mathbb{P}(L - h, h):\mathbb{P}(L - 2h, h):\ldots\mathbb{P}(2h, h):\mathbb{P}(h, h):\mathbb{P}(0, h) \tag{10}$$

$$\mathbb{P}(z, h) = \mathbb{P}_0(h) + [\mathbb{P}_0(h):\mathscr{D}_2(z)]\left(\frac{h\omega}{c}\right) \approx \mathbb{P}_0(h) + \left(\frac{h\omega}{c}\right)\mathscr{D}_2(z) \tag{11}$$

$$\mathscr{D}_2(z) = \begin{pmatrix} 0 & 0 & 0 & 0 \\ -\delta\cos 2\beta z & 0 & -\delta\sin 2\beta z & 0 \\ 0 & 0 & 0 & 0 \\ -\delta\sin 2\beta z & 0 & +\delta\cos 2\beta z & 0 \end{pmatrix} \tag{12}$$

$$\mathbb{P}_0(h) = \begin{pmatrix} \cos(abh\omega/c) & (a/b)\sin(abh\omega/c) & 0 & 0 \\ (-b/a)\sin(abh\omega/c) & \cos(abh\omega/c) & 0 & 0 \\ 0 & 0 & \cos(vh\omega/c) & (1/v)\sin(vh\omega/c) \\ 0 & 0 & (-v)\sin(vh\omega/c) & \cos(vh\omega/c) \end{pmatrix} \tag{13}$$

$$a = \left[1 - \frac{(k \times c/\omega)^2}{\epsilon_z}\right]^{1/2}$$

$$b = (\bar{\epsilon})^{1/2}$$

$$v = \left[\bar{\epsilon} - \left(\frac{k_x c}{\omega}\right)^2\right]^{1/2} \tag{14}$$

and $h$ is the length of a differential incremental step. Since the surface plasmon wave is physically confined to a narrow region of $\sim\lambda/\pi$ around the interface, we actually have $\mathbb{F}(0, L) \simeq \mathbb{F}(0, z)$ for $z \gtrsim \lambda$.

Since $\theta_1$ is above the critical angle, normally the incoming beam is totally reflected, but when $\theta_1$ approaches a value that makes the real part of the denominator in Eq. (5) vanish

$$\mathrm{Re}\{[1 + \gamma_{12}^{pp}\gamma_{23}^{pp}\exp(i2k_{2z}d)][1 + \gamma_{12}^{ss}\gamma_{23}^{ss}\exp(i2k_{2z}d)] - \gamma_{12}^{pp}\gamma_{12}^{ss}\gamma_{23}^{ps}\gamma_{23}^{sp}\exp(i4k_{2z}d)\} = 0 \tag{15}$$

the reflectivity $R(\theta_1)$ drops drastically. Physically, this corresponds to the excitation of the surface plasmon and Eq. (15) describes the surface plasmon dispersion relation. The width of the reflectivity dip is proportional to the damping coefficient of the surface plasmon. Knowing the wavelength of light, the thickness and optical constants of the metal film, the pitch of the cholesteric structure, the entire reflectivity curve can be calculated from Eqs. (5)–(14) if the optical constants of the liquid crystal are given. Conversely, from the theoretical fit to the experimental reflectivity curve, the optical constants of the liquid crystal can be deduced. Here, we use the latter procedure to find the refractive indices of the cholesteric liquid crystal.

## III EXPERIMENTAL ARRANGEMENT AND PROCEDURE

The experimental arrangement has been described in Ref. 9. The assembly in Figure 1 in the present case was composed of a glass prism with a high refractive index (Schott glass LaSF6 with $n = 1.9549$), a silver metal film of $\sim 500$ Å evaporated on the prism, and a $\sim 50$ $\mu$m layer of cholesteric liquid crystal sandwiched between the silver film and a glass plate. To align the cholesteric molecules along $\hat{y}$ on the boundary surfaces, $a \sim 100$ Å film of SiO was obliquely evaporated at 60° onto the silver film and the glass plate.

The sample was a 1.75:1.00 mixture of cholesteryl chloride and cholesteryl myristate. The materials were obtained from Aldrich Co. and Eastman Co. and used without further purification. The sample assembly was inserted in a two-stage temperature-controlled oven, which in turn was mounted on a rotating stage driven by a stepping motor. During a 15 min. scan of the reflectivity curve, the temperature stability could be better than 1 mK. The light source was a 0.5–mW CW He-Ne laser and the reflected beam was detected by a silicon photodiode. A Tektronix 4051 minicomputer was used to control the stepping motor, record the intensity of the reflected beam as a function of the angular position of the sample cell, and normalize the reflected beam intensity against the incident beam intensity to yield reflectivity.

## IV RESULTS

Typical reflectivity curves at $T < T_c$ and $T > T_c$ are shown in Figure 2 where $T_c$ is the isotropic-cholesteric transition temperature. To find the local refractive indices $n_{\parallel}$ and $n_{\perp}$, Eqs. (5)–(14) were used to fit the reflectivity curves. In the calculation, however, it is necessary to know the pitch value of the cholesteric structure. We used the diffraction method[18] with the help of a He-Ne laser to measure the pitch. The result as a function of temperature is shown in Figure 3. The numerical calculation using Eqs. (5)–(14) and a nonlinear least-square program was then carried out to fit the experimental results and deduce $n_{\parallel}$ and $n_{\perp}$. The theoretical fit is shown as solid curves in Figure 2. The values of the thickness and optical constants of the silver film, also required in the calculation, were on the other hand deduced from the fit to a reflectivity curve in the isotropic phase, knowing the value of the refractive index of the isotropic liquid from a separate critical angle measurement (discussed later).

The local refractive indices $n_{\parallel}$ and $n_{\perp}$ in the quasi-nematic layer of the cholesteric liquid crystal thus obtained are shown in Table I and Figure 4. The accuracy of these $n$ values is $\sim 10^{-4}$, and was limited by the angular resolution of our apparatus (0.01°). It is relatively insensitive to the pitch

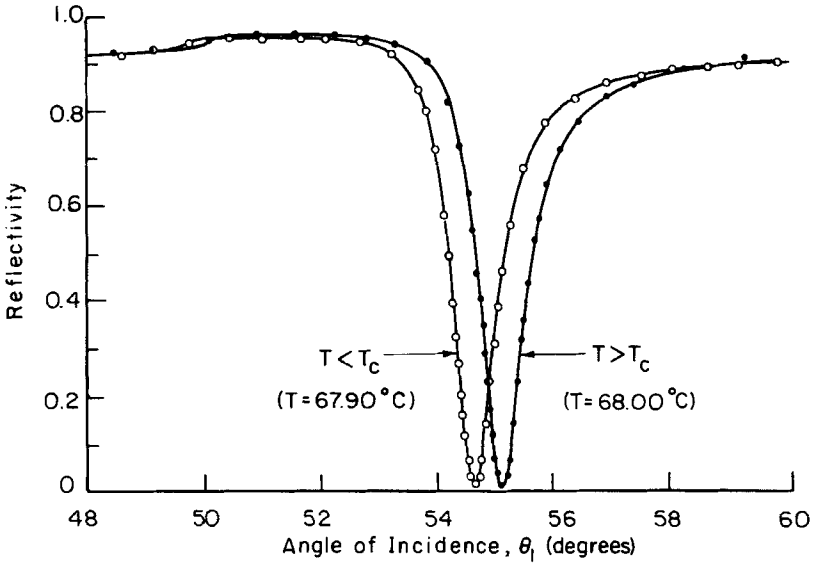


FIGURE 2 Reflectivity curves versus the angle of incidence $\theta_1$ at $T < T_c$ and $T > T_c$. The solid curves are theoretical curves obtained by nonlinear least square fitting.

value since the penetration depth of the surface plasmon wave into the liquid crystal side is only a small fraction of the pitch. The imaginary parts of $n_{\parallel}$ and $n_{\perp}$ were found to be less than $10^{-4}$ and can therefore be neglected in the theoretical fit.

The orientational order parameter is one of the most important quantities of a liquid crystal. For the cholesteric phase, we are interested in the molecular orientational ordering within a quasi-nematic layer. The corresponding order parameter can be represented by the local linear birefringence $\Delta n = n_{\parallel} - n_{\perp}$ in the quasi-nematic layer. In Figure 5, we plot the temperature dependence of $\Delta n(T)$. As expected, the behavior of $\Delta n(T)$ is very similar to those of nematics. It is also similar to the results[19] of the order parameter $S(T)$ obtained from NMR measurements on a cholesteric liquid crystal, even though the samples used in the two cases are different.

In passing, we note that in the literatures,[2-5] the mean ordinary and extraordinary refractive indices $n_0$ and $n_e$ of a cholesteric liquid crystal are often used. They are related to $n_{\parallel}$ and $n_{\perp}$ by the relations[3]

$$n_e = n_{\perp}$$
$$n_0 = \sqrt{(n_{\parallel}^2 + n_{\perp}^2)/2}. \tag{16}$$

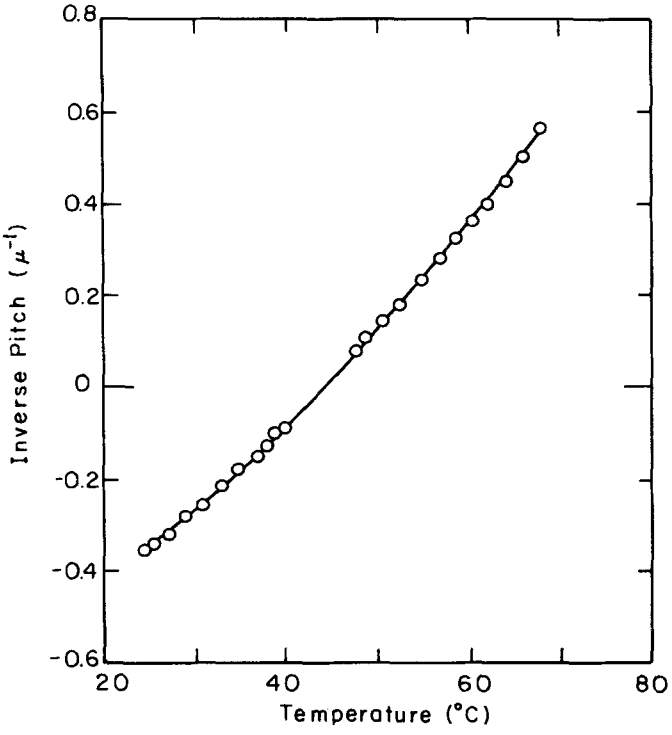


FIGURE 3 Variation of the inverse pitch ($1/P$) with temperature for the mixture of 1.75 cholesteryl chloride and 1 cholesteryl myristate. The experimental uncertainty is $\pm 0.005\ \mu m^{-1}$. The solid line is an approximate fit to the experimental points.

## V DISCUSSION

It is commonly believed that the cholesteric structure can be regarded as a twisted nematic, or a nematic is a special case of cholesterics with an infinite pitch. Thus, the molecular orientational ordering of a cholesteric in the planes perpendicular to the helical axis should resemble that of a nematic in the bulk, and the theory of molecular ordering for a nematic should apply equally well to the molecular ordering in the quasi-nematic layers of a cholesteric. As mentioned earlier, the local birefringence $\Delta n$ (after normalization) can be used as the orientational order parameter for molecules in the quasi-nematic layers. We can therefore compare the experimental results in Figure 5 with the theoretical models for nematic ordering. This is shown in Figure 6, where the solid curve was obtained from the Maier–Saupe mean field theory[20] and the dashed curve from the improved theory of Humphries,

James, and Luckhurst (HJL).[21] The latter is in excellent agreement with our results. As a comparison between cholesterics and nematics, we have also plotted in Figure 6 the order parameter results of anisaldalzine from the optical anisotropy measurements[22] and MBBA from the Raman scattering measurements.[23] The good agreement of these different sets of data with the theoretical curve of HJL indicate that first, the HJL theory is a valid description of the nematic ordering, and second, the molecular ordering in the planes perpendicular to the helical axis of a cholesteric is indeed nematic.

The advantages of the surface plasmon technique for measuring refractive indices of cholesterics are numerous. It can determine the local $n_{\parallel}$ and $n_{\perp}$ separately. The accuracy can be better than $10^{-4}$. Since the surface plasmon wave does not penetrate more than a fraction of a pitch length into the liquid crystalline medium, the result is rather insensitive to the helical structure of the cholesteric. Consequently, the method can be used to measure refractive indices at wavelengths in and out of the Bragg reflection band ($\lambda \sim p$). Also, in this technique, the sample thickness need not be known as long as it is larger than a wavelength.

TABLE I

Refractive indices of a 1.75:1.00 by weight cholesteryl chloride/cholesteryl myristate mixture versus temperature ($\lambda$ = 6328 Å)

| Temperature (°C) | $n_{\parallel}$ | $n_{\perp}$ | Method |
|---|---|---|---|
| 36.20 | 1.5462 | 1.4992 | a |
| 40.00 | 1.5442 | 1.4975 | a |
| 41.60 | 1.5430 | 1.4970 | a |
| 45.71 | 1.5408 | 1.4953 | a |
| 49.63 | 1.5381 | 1.4942 | a |
| 50.02 | 1.5376 | 1.4938 | b |
| 51.64 | 1.5365 | 1.4936 | a |
| 53.66 | 1.5346 | 1.4931 | a |
| 55.65 | 1.5330 | 1.4927 | a |
| 57.91 | 1.5306 | 1.4923 | a |
| 59.80 | 1.5284 | 1.4920 | a, b |
| 61.90 | 1.5263 | 1.4915 | a |
| 63.90 | 1.5237 | 1.4913 | a |
| 65.93 | 1.5204 | 1.4915 | a |
| 66.89 | 1.5183 | 1.4920 | a |
| 67.90 | 1.5155 | 1.4922 | a, b |
| 68.00 | 1.5000 | | a |
| 69.02 | 1.4996 | | a |
| 72.17 | 1.4982 | | a |
| 77.12 | 1.4960 | | a, b |

[a] surface plasmon method.
[b] critical angle method.

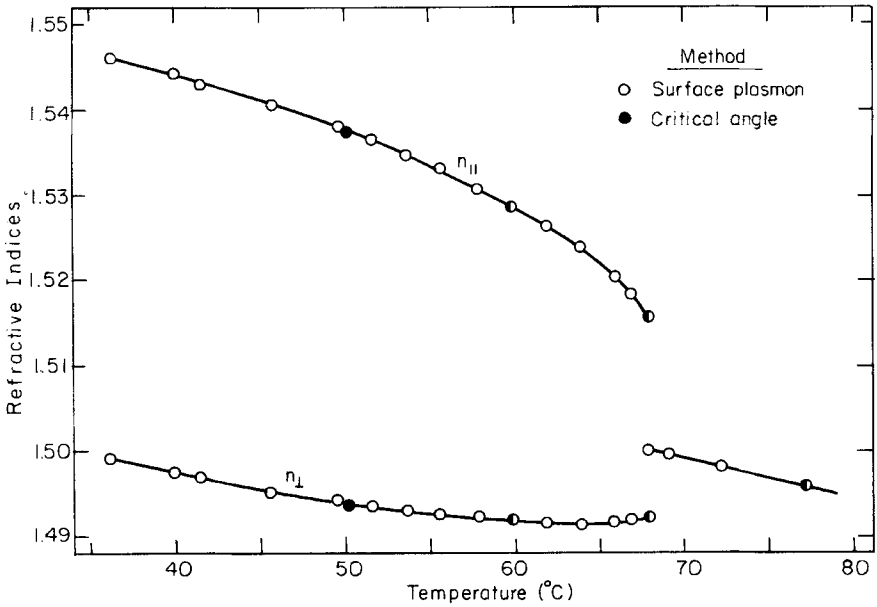


FIGURE 4 Refractive indices of the mixture of 1.75 cholesteryl chloride and 1 cholesteryl myristate versus temperature. ● obtained by the critical angle method; ○ obtained by the surface plasmon technique.

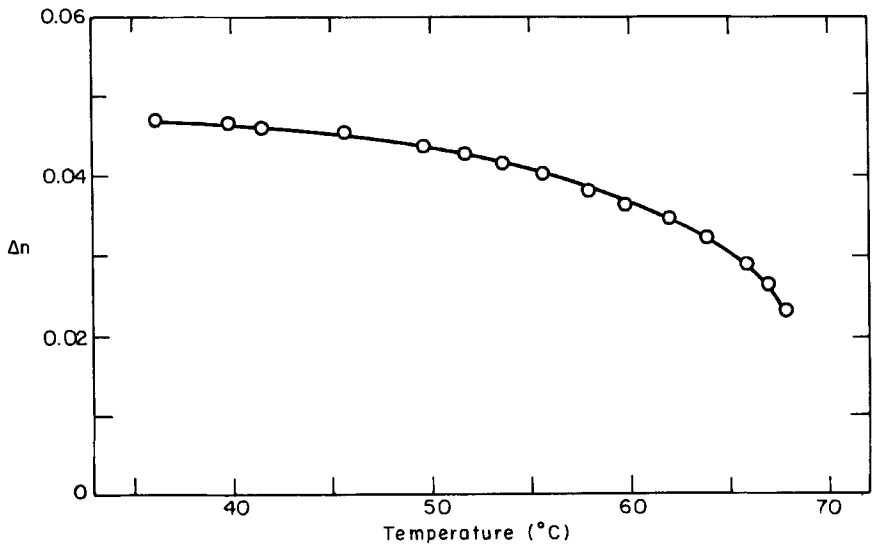


FIGURE 5 Local linear birefringence $\Delta n = n_{\parallel} - n_{\perp}$ of the mixture of 1.75 cholesteryl chloride and 1 cholesteryl myristate as a function of temperature.

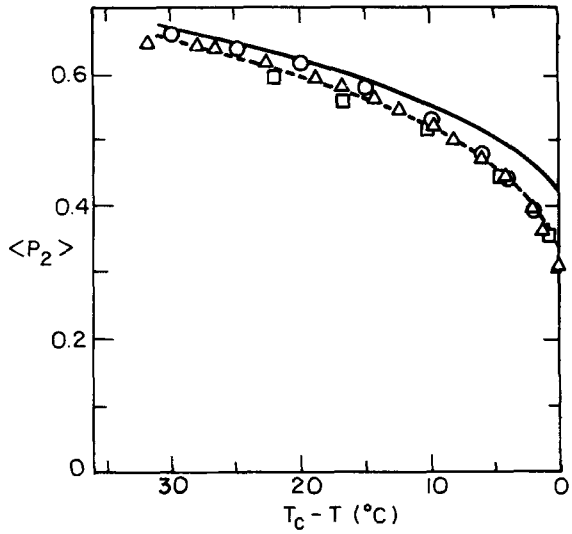


FIGURE 6 Theoretical and experimental order parameters $\langle P_2 \rangle$ versus temperature: the solid line is obtained from the Maier-Saupe theory and the dashed line from the Humphries-James-Luckhurst theory with parameters $\lambda = -0.55$ and $\gamma = 10$. Squares are values deduced from measurements of optical anisotropy of anisaldazine in the nematic phase. Open circles are results from Raman scattering in MBBA. Triangles are normalized $\Delta n$ values given in Figure 5 for the cholesteric mixture.

In comparison, the optical rotatory dispersion (ORD) and circular dichroism (CD) methods are much less accurate. The ORD method measures the optical rotation of light propagating along the helical axis. It is simple in arrangement and in reduction of data, but it yields only the linear birefringence $\Delta n$ and cannot be used if the optical wavelength is within the reflection band. Far away from the reflection band, its accuracy is limited by the elastic scattering background and rotation angle measurement[6,7] to $\sim 5 \times 10^{-3}$. The CD method measures the circular dichroism spectrum of the reflection band, and $n_{\parallel}$ and $n_{\perp}$ averaged over the frequencies of the reflection band is deduced from the theoretical fit to the measured spectrum. Therefore, it cannot be used to find the dispersion of $n_{\parallel}$ and $n_{\perp}$, and the accuracy is expected to be about the same as the ORD method. Another simple method for measuring refractive indices of cholesterics is to use the Abbe refractometer. Basically, the refractometer locates the critical angle for total reflection, and the ordinary and extraordinary refractive indices ($n_0$ and $n_e$) can be obtained from direct reading, assuming that the refractive indices are spatially invariant. The assumption is of course not true for cholesterics, so that the result is only an approximation which becomes progressively worse as the helical pitch length decreases. As an example, for a 1 $\mu$m pitch, the error in the measured refractive indices is about $10^{-3}$.

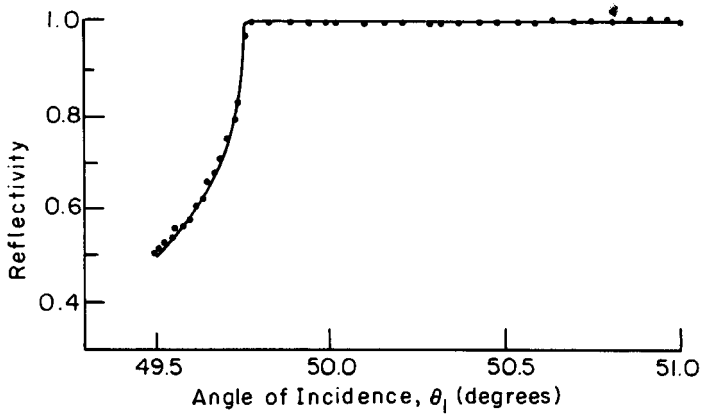


FIGURE 7 Reflectivity versus incidence angle around the critical angle with polarization in the plane of incidence for the mixture of 1.75 cholesteryl chloride and 1 cholesteryl myristate at $T = 67.90°C$. The solid curve is a theoretical fit.

The Abbe refractometer method can of course be improved by first recording carefully the entire reflectivity curve around the critical angle,[24] and then, using a theoretical calculation similar to that discussed in Section II which takes into account the spatial variation of the helical structure to fit the measured reflectivity curve. The measurement can actually be done on the same setup for the surface plasmon work, and the computer program for the numerical calculation is also essentially the same. An example is shown in Figure 7, and the local refractive indices $n_{\parallel}$ and $n_{\perp}$ obtained from the theoretical fit to the measured reflectivity curves at a number of temperatures are given in Figure 4 and Table I. They agree very well with those obtained from the surface plasmon method. The critical angle method discussed here seems to have all the advantages of the surface plasmon method. A glance at Figures 2 and 7 however suggests that the surface plasmon method should be more accurate. The reason is that the optical field penetrates deeper and deeper into the liquid crystalline medium as the incident angle $\theta_1$ decreases and approaches the critical angle. The effect of the helical structure of the medium then becomes more important. Below the critical angle, interference due to multiple reflections at the prism-liquid crystal, the liquid crystal-glass plate, and the glass plate-air boundaries also occurs. All these make the theoretical calculation more complicated and the fit to the measured curve more difficult. As a result, with the same angular resolution in the measurement and the same mean square deviation in the fit, the accuracy of the critical method is 2–3 times less than the surface plasmon method.

Because of the high sensitivity of the surface plasmon technique, it can be used to probe small changes in the refractive indices, and hence the details of the phase transition behavior of a liquid crystal. This was first tried out on a nematic in Ref. 9. Coexistence of nematic and liquid phases over a 60 mK range around the isotropic-nematic transition was observed. In the present experiment, however, we have not been able to find a similar coexistence region around the isotropic-cholesteric transition. It is most likely that the aligned single domain in the cholesteric phase may have broken into randomly oriented multi-domains before the transition actually takes place. We have observed that the plane texture of the cholesteric has a tendency to become focal conic, and it can be maintained only if the temperature variation is slow and the cover glass plate is shifted back and forth with respect to the prism for a number of times.

## VI CONCLUSION

The surface plasmon technique discussed here can be applied in general to all kinds of liquid crystals. For cholesterics, the theoretical calculation of the reflectivity is somewhat more complicated because of the helical structure of the medium. Nevertheless, the local refractive indices in the quasi-nematic layers can be deduced from the theoretical fit to the measured reflectivity curve with an accuracy about $10^{-4}$. Variations of the local refractive indices and linear birefringence with temperature have been studied. They show the characteristic behavior of a nematic with an abrupt change at the cholesteric-isotropic transition. With the local linear birefringence $\Delta n$ representing the order parameter of molecules in the quasi-nematic layers, the result of $\Delta n$ versus $T$ after proper normalization can be compared with both theory and experiment of the temperature variation of the order parameters of nematics. The agreement is excellent, confirming the belief that a cholesteric can be regarded as a twisted nematic. In comparison with other techniques, the surface plasmon technique has clear advantages and yields better accuracy.

## References

1. I. Haller, *Progress in Solid State Chemistry*, **10**, 103 (1975), and references therein.
2. B. Böttcher and G. Graber, *Mol. Cryst. Liq. Cryst.*, **14**, 1 (1971).
3. W. U. Müller and H. Stegemeyer, *Ber. Bunsenges. Phys. Chem.*, **77**, 20 (1973).
4. P. Adamski and A. Dylik-Gromiec, *Mol. Cryst. Liq. Cryst.*, **25**, 273 (1974).
5. P. Adamski and A. Dylik-Gromiec, *Mol. Cryst. Liq. Cryst.*, **25**, 281 (1974).
6. J. W. Shelton and Y. R. Shen, *Phys. Rev. Lett.*, **25**, 23 (1970).
7. I. Teucher, K. Ko, and M. M. Labes, *J. Chem. Phys.*, **56**, 3308 (1972).

8. A. V. Tolmachev, V. G. Tishchenko, and L. N. Listeskii, *Sov. Phys. Solid State*, **19**, 1105 (1977); *Sov. Phys. JETP*, **48**, 333 (1978).
9. K. C. Chu, C. K. Chen, and Y. R. Shen, *Mol. Cryst. Liq. Cryst.* (to be published).
10. G. Borstel and H. J. Falge, *Appl. Phys.*, **16**, 211 (1978), and references therein.
11. E. Kretschmann, *Zeit. Phys.*, **241**, 313 (1971).
12. A. Otto in *Optical Properties of Solids, New Developments*, ed. by B. O. Seraphin (North-Holland, Amsterdam, 1976), p. 677.
13. J. G. Gordon and J. D. Swalen, *Optics Comm.*, **22**, 374 (1977).
14. W. H. Weber, *Phys. Rev. Lett.*, **39**, 153 (1977).
15. C. W. Oseen, *Trans. Faraday Soc.*, (G.B.) **29**, 833 (1933).
16. D. Taupin, *J. de Physique*, **30**, C4–32 (1969).
17. D. W. Berreman and T. J. Scheffer, *Phys. Rev. Lett.*, **25**, 577 (1970); see also *Mol. Cryst. Liq. Cryst.*, **11**, 395 (1970).
18. E. Sackman, S. Meiboom, L. C. Snyder, A. E. Meixner, and R. E. Dietz, *J. Am. Chem. Soc.*, **90**, 3567 (1968).
19. P. J. Collins, T. J. McKee, and J. R. McColl, *J. Chem. Phys.*, **65**, 3520 (1976).
20. W. Maier and A. Saupe, *Z. Naturforsch.*, **13a**, 564 (1958); **14a**, 882 (1959); **15a**, 287 (1960).
21. R. L. Humphries, P. G. James, and G. R. Luckhurst, *J. Chem. Soc. Faraday Trans II*, **68**, 1031 (1972).
22. N. V. Madhusudana, R. Shashidhar, and S. Chandrasekhar, *Mol. Cryst. Liq. Cryst.*, **13**, 61 (1971); S. Chandrasekhar and N. V. Madhusudana, *J. de Phys.*, **30**, C4–24 (1969).
23. P. S. Pershan in *Theory of Light Scattering in Condensed Matter*, ed. by B. Bendow, J. L. Birman, and V. M. Agranovich (Plenum, New York, 1976), p. 53.
24. D. Riviere, Y. Levy, and C. Imbert, *Opt. Comm.*, **25**, 206 (1978).